Applied Energy 204 (2017) 497–508

Contents lists available at ScienceDirect

Applied Energy

journal homepage: www.elsevier.com/locate/apenergy

On-line scheme for parameter estimation of nonlinear lithium ion battery equivalent circuit models using the simplified refined instrumental variable method for a modified Wiener continuous-time model

Walid Allafi [a,*], Kotub Uddin [a], Cheng Zhang [a], Raja Mazuir Raja Ahsan Sha [b], James Marco [a]

[a] WMG, The University of Warwick, Coventry CV4 7AL, United Kingdom
[b] Charge Auto, Oxford Industrial Park, Cassington Road, Yarnton, Oxfordshire OX5 1QU, United Kingdom

HIGHLIGHTS

- Off-line estimation approach for continuous-time domain for non-invertible function.
- Model reformulated to multi-input-single-output; nonlinearity described by sigmoid.
- Method directly estimates parameters of nonlinear ECM from the measured-data.
- Iterative on-line technique leads to smoother convergence.
- The model is validated off-line and on-line using NCA battery.

ARTICLE INFO

Article history:
Received 31 March 2017
Received in revised form 30 June 2017
Accepted 15 July 2017
Available online 25 July 2017

Keywords:
Lithium ion battery
Nonlinear equivalent circuit model
Online parameter estimation
Continuous time wiener model
Simplified refined instrumental variable method

ABSTRACT

The accuracy of identifying the parameters of models describing lithium ion batteries (LIBs) in typical battery management system (BMS) applications is critical to the estimation of key states such as the state of charge (SoC) and state of health (SoH). In applications such as electric vehicles (EVs) where LIBs are subjected to highly demanding cycles of operation and varying environmental conditions leading to non-trivial interactions of ageing stress factors, this identification is more challenging. This paper proposes an algorithm that directly estimates the parameters of a nonlinear battery model from measured input and output data in the continuous time-domain. The simplified refined instrumental variable method is extended to estimate the parameters of a Wiener model where there is no requirement for the nonlinear function to be invertible. To account for nonlinear battery dynamics, in this paper, the typical linear equivalent circuit model (ECM) is enhanced by a block-oriented Wiener configuration where the nonlinear memoryless block following the typical ECM is defined to be a sigmoid static nonlinearity. The nonlinear Weiner model is reformulated in the form of a multi-input, single-output linear model. This linear form allows the parameters of the nonlinear model to be estimated using any linear estimator such as the well-established least squares (LS) algorithm. In this paper, the recursive least square (RLS) method is adopted for online parameter estimation. The approach was validated on experimental data measured from an 18650-type Graphite/Lithium-Nickel-Cobalt-Aluminium-Oxide (C_6/$LiNiCoAlO_2$) lithium-ion cell. A comparison between the results obtained by the proposed method and by nonparametric frequency-based approaches for obtaining the model parameters is presented. It is shown that although both approaches give similar estimates, the advantages of the proposed method are (i) the simplicity by which the algorithm can be employed on-line for updating nonlinear equivalent circuit model (NL-ECM) parameters and (ii) the improved convergence efficiency of the on-line estimation.

1. Introduction

Effective real-time control of LIB systems relies on efficient estimations of the state of charge (SoC) and state of health (SoH). This

* Corresponding author.
E-mail address: W.Allafi@warwick.ac.uk (W. Allafi).

http://dx.doi.org/10.1016/j.apenergy.2017.07.030
0306-2619/

Nomenclature

BMS	battery management system
ECM	equivalent circuit model
EIS	electrochemical impedance spectroscopy
EV	electric vehicle
KF	Kalman filter
LIB	lithium ion battery
LS	least squares
NL-ECM	nonlinear ECM
OCV	open circuit voltage
RC	resistor-capacitor
RLS	recursive least squares
SoC	state of charge
SoH	state of health
Wm	Wiener model
WSRIV	simplified refined instrumental variable for Wiener model

in turn, depends on operating conditions and usage, particularly the frequency of cycling as well as the complex interactions between voltage, current, temperature and depth of discharge [1–3] during both cycling and storage [4–7]. State estimation is especially important for applications such as electric vehicles (EVs) where the inaccurate estimation of SoC and SoH can lead to over-charge or over-discharge events with significant implications for system safety and reliability [8]. As such, Battery Management Systems (BMS) typically employ physical models to estimate the states of a given battery through the model parameters [9–13] . To this end, there has been a large body of work focusing on developing methods of estimating LIB model parameters for use within real-time operation. This includes, for example, least square methods [14–18], state observer and adaptive observer techniques [15], [17–19], support vector machines [20] and genetic algorithms [21].

Fleischer et al. [22] summarised the most commonly used methods for on-line estimation LIB model parameters into three subgroups: methods using electrochemical impedance spectroscopy (EIS), methods employing ECMs and methods based on electrochemical models. EIS methods such as that proposed by Howey et al. [23], [24], where it's argued that the harmonics generated by the electric motor connected to the EV powertrain can be harnessed to estimate the EIS and hence battery impedance. The challenge in this case, in addition to the requirement for bespoke electronics which may be prohibitively expensive, is the limited range of excitation frequencies present [22]. Furthermore, apart from cell impedance, it is not obvious how EIS can be used to define other important metrics such as the SoC, SoH and cell capacity. The second subgroup of parameter estimation methods is based on traditional linear ECMs [22]. To identify the unknown model parameters and states, various implementations of the least squares (LS) method have been applied to estimate the best solution of an overdetermined system which minimises the sum of squared residuals [22]. The variations of LS filters include the RLS filter and the weighted RLS filter [25–32]. Non-recursive filters such as batch learning [33,34], which also employ an iterative LS procedure, enable the estimation of NL-ECM parameters, although this is at a cost of higher memory and computing resource [22]. Furthermore, with such non-recursive filters, high frequency real-time parameters may evolve during the evaluation procedure and therefore may not be up-to-date with the corresponding operating point [22]. More accurate but computationally expensive filters for parameter estimation are based on different implementations of the Kalman filter (KF). The KF is a recursive procedure which combines analytical and probabilistic Bayesian models. Although the assumption of linearity and Gaussian noise in typical KFs are applicable to a wide class of problems, for highly nonlinear model equations such as the case for LIBs, generalisations of the KF are required. Such generalisations include: the dual extended KF [35–37] which consists of two different extended KFs in which the results are calculated in parallel; the joint extended KF [38,39] where model parameters are re-adapted at the same time, thus increasing computing effort due to the higher dimensional model matrices [22]; the dual sigma-point KF [35]; the joint sigma-point KF [40]; and the particle filter [41]. Although KF based approaches may be more accurate, the computational cost is known to be significantly higher due to the required matrix inversions which may lead to numerical instability. To take into consideration both the nonlinearity of models and the uncertainties and noise in measurements, nonlinear and robust observers such as H-infinite filters [42,43] and sliding mode observers [44–46] have been applied for battery parameters and state estimation.

Both LS and KF methods have been applied to electrochemistry based battery models [5,47–50] for estimating model parameters. The complex calculations of the models themselves, let alone the adaptive filters, render the applicability of such techniques challenging for many commercial BMS's that employ low-cost microcontrollers. Furthermore, as discussed in Refs. [5,47], the relatively large number of model parameters associated with electrochemical battery models means that parameters are seldom uniquely identifiable. A more detailed review and discussion of commonly used methods for parameter and state estimation are beyond the scope of this work, interested readers are directed to Ref. [22].

Although ECMs are comparatively simple and require less computational effort to evaluate [1], [51], they are unable to capture important dynamics such as solid phase diffusion limitation resulting from large current loads or low ambient temperatures [52]. Electrochemical models on the other hand, which have a recognisable correspondence with electrochemistry, can readily accommodate solid phase diffusion [52] – at the expense of extra computational resource, however. The trade-off between model accuracy and computational resource adopted in this work is to consider a Weiner configuration cascade of an ECM coupled with a nonlinear overpotential correction function. The latter is motivated by the Butler-Volmer relation and accommodates for the nonlinear voltage response generated by high current densities and/or low temperatures [53]. In the context of real applications, the advantages of the Hammerstein/Wiener/Hammerstein-Wiener class of nonlinear models include: (i) that the dynamics of systems are mainly generated by the linear subsystem so that algorithms and techniques developed for the linear systems may be adopted for the Hammerstein/Wiener model and (ii) if the static nonlinearity has an inverse function, such that it allows for a cancellation with the static nonlinearity, then linear control algorithms can be applied. Thus, the adopted Weiner model in this paper can capture the nonlinear dynamics of a LIB while still maintaining a simple model structure with low complexity allowing a suitably simple online estimation technique to be adopted.

The estimation approach of the Wiener models can either be categorised as iterative or non-iterative. This work has primarily focused on iterative methods. In the discrete time-domain, the iterative algorithm proposed in [54] is based on accessing the internal signals by using the key term separation principle as a decomposition technique. This algorithm was extended for the case of multi-inputs by Vörös in [55]. The approach adopted in [54,55] express

the Hammerstein and Wiener models in a linear-in-the-parameter manner. The key term separation principle and estimated linear outputs, adopted in [54,55], are also used in the case of the Wiener model in [56]. The principle drawbacks of this approach are namely, that it is not a direct identification method and the convergence is not guaranteed. Other approaches for discrete iterative methods can be found in [57]. In recent studies in the discrete domain, the kernel, Volterra and fractional least mean square algorithms have been applied for estimating the parameters of the Hammerstein models associated with coloured noise process [58]. These approaches were able to estimate the model parameters but required a large number of iterations. Although the iteration number was shown to be reduced by employing the sliding-window approximation-based fractional least mean squares in [59], still, the iteration number is considerably large. The aforementioned approaches are all in the discrete-time domain and are employed for obtaining the continuous-time transfer function of the linear subsystem. A further step is required to convert from the discrete-time to the continuous-time domain and this class of estimation approaches is termed indirect.

The contributions of this paper are summarised as follows. Firstly, a nonlinear Weiner-type battery model, consisting of a linear ECM and a new static sigmoid block – motivated by the Bulter-Volmer equation – is proposed. In addition to capturing nonlinear battery dynamics, the model also maintains a simple structure and low complexity. Secondly, the proposed estimation method directly estimates the parameters of the nonlinear model from the measured data (current and voltage), while previous methods were nonparametric [60] and limited to off-line estimation. Thirdly, the model equations are reformulated into a *linear-in-the-parameter* form using the instrumental variables technique. This then lends itself for nonlinear model parameter identification using any linear estimator, such as the well-established LS algorithm. In this way, the computational efficiency of the LS method can be capitalised without loss of model fidelity. Fourthly, the classical form of the *simplified refined instrumental variable* method (SRIVC) is extended to the *simplified refined instrumental variable for Wiener model* (WSRIVC) *in* the continuous-time domain for non-invertible static nonlinearity. This is then applied off-line to estimate model parameters. Fifthly, the proposed WSRIVC method is extended from an iterative off-line to an iterative on-line method in a recursive manner for parameter identification in real time. For this, the estimation step is decoupled into linear and nonlinear sub-estimations to ensure the stability of estimator. This extension increases the applicability of the algorithm to real-time applications where the model parameters within the look-up table need to be updated due to battery degradation. Finally, original test data is collected for commercial Li-ion NCA cells under various temperatures and SOC conditions.

This paper is structured as follows: background on the structure and parameter estimation technique is presented in Section 2. The problem description in terms of the Wiener sub-model (Wm) of the NL-ECM and problem reformulation based on Wm are then addressed in Section 3 and 4, respectively. Furthermore, the derivation of the WSRIVC method for the selected nonlinearity is given in Section 5, which is then extended to the on-line parameter estimation in Section 6. Section 7 presents and discusses the obtained results. Section 8 presents the conclusions and further work from this research.

2. Background of nonlinear battery model and parameter estimation

The NL-ECM model adopted in this work is presented in Fig. 1 and consists of three elemental blocks, i.e., an ECM, a nonlinear

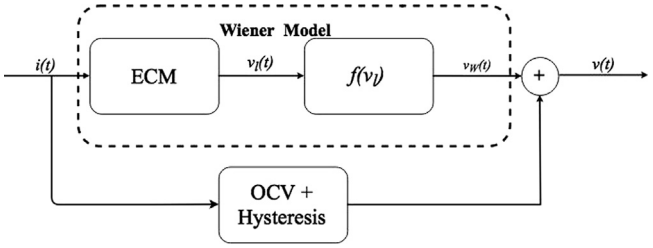

Fig. 1. The block diagram of the NL-ECM.

over-voltage function $f(v_l)$ and an open circuit voltage (OCV) coupled with hysteresis [53]. The OCV represents the equilibrium potential of the system, i.e., the potential difference between the negative and positive electrodes when no current is applied and the system is at rest. Hysteresis on the other hand accounts for differences observed in OCV measurements depending on the path taken to a particular state, i.e., whether the particular SoC was reached via a charge or discharge [60]. Hysteresis is related to thermodynamic entropic effects, mechanical stress, and microscopic distortions within the active electrode materials following the application of an electrical load [61], [62].

The ECM, shown in Fig. 2 [63], characterises the dynamics of the battery. The model structure comprises of two parallel resistor–capacitor (RC) networks connected in series with a resistor. Each circuit element represents a particular phenomenon governed by its respective timescales. The pure Ohmic resistance R_0 comprises all electronic resistances of the battery and corresponds to the instantaneous voltage drop when a battery is connected to an electrical load. The charge transfer process which is attributed to the charge transfer reaction at the electrode/electrolyte interface and the double layer capacitance [3] is captured by R_{p1} and C_{p1} and typically corresponds to a frequency (f) of $f \geqslant 1Hz$. Ionic diffusion in the solid phase is represented by R_{p2} and C_{p2} and is usually characterised in pulse power tests as the linear (or close to linear) voltage drop and corresponds to a frequency of between $0.001Hz \leqslant f \leqslant 1Hz$. Solid phase ionic diffusion is usually considered to be the rate determining step for Li ion batteries [52]. It is noteworthy that the ECM structure presented in this paper neglects the high frequency inductive behaviour of the battery, which is known to occur at much higher frequencies, e.g., $f > 300$ Hz and is therefore beyond the frequency range associated with most battery management control systems.

The linear kinetics of the LIB is phenomenologically modelled in this paper using an ECM. Nonlinearity associated with current density comprises of concentration polarisation and active polarisation, which is dominant [52]. In classical electrochemistry, concentration polarisation is described by Fick's diffusion equation

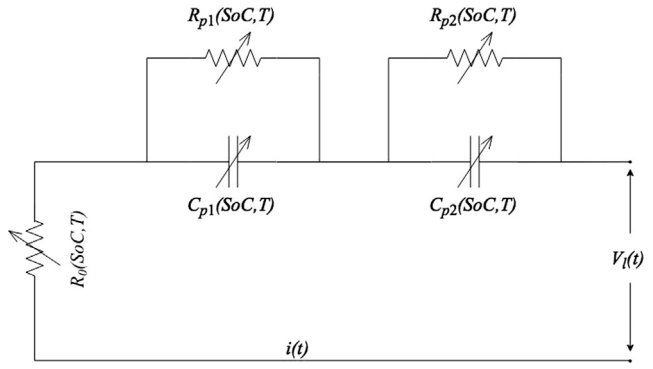

Fig. 2. The linear ECM.

while the reaction kinetics of the battery (and thus active polarisation) is modelled by the Butler-Volmer equation:

$$i_d = i_0\left\{\exp\left[\frac{\alpha_a F}{RT}\eta\right] - \exp\left[\frac{\alpha_c F}{RT}\eta\right]\right\} \tag{1}$$

where i_d, η, i_0, T, F,R,α_a and α_c represent the current density, over-potential, exchange current density, temperature, Faraday constant, the universal gas constant, and the anodic and cathodic exchange coefficients, respectively. Eq. (2) combines two Tafel expressions of the form

$$\eta = a + b\log(i_d) \tag{2}$$

to handle the forward and reverse reaction rates that occur at the electrode–electrolyte interface. The parameters a and b in Eq. (2) are constants, typically defined through fitting to constant current discharge curves. The Tafel expressions skew the forward or reverse reaction depending on the sign of the applied over-potential [64]. In the high over-potential regime, i.e. the Tafel regime, the Faradic reaction kinetics are nonlinear [65]. This nonlinearity is captured in the equivalent circuit formulation by a nonlinear over-voltage function $f(v_l)$ and takes the form [53]:

$$f(v_l) = \frac{c_1 v_l(t)}{1 + c_2\|v_l(t)\|} \tag{3}$$

where $v_l(t)$ is the linear over-voltage signal and c_1 and c_2 are sigmoid coefficients that need to be estimated. Derivation of $f(v_l)$ as well as further discussion on the form of $f(v_l)$ can be found in [53], [66]. The Weiner sub-model is described in the following section.

3. Problem description for the Wiener sub-model

This section describes the Wm for the NL-ECM shown in Fig. 1. The Wm is a cascade of the ECM and the nonlinear over-voltage function that represents the continuous-time linear model and output static nonlinear function, in the classical Weiner formulation respectively. The input to the Wm is the load current $i(t)$ and the output is the Wiener voltage, denoted by $v_W(t)$, as shown in Fig. 1. The NL-ECM can be described by three input-output relationships as follows:

$$\begin{aligned} v_l(t) &= \tfrac{B(\mathcal{D})}{A(\mathcal{D})} i(t) \\ v_W(t) &= \tfrac{c_1 v_l(t)}{1+c_2\|v_l(t)\|} \\ v(t) &= v_w(t) + v_{OCV}(t) + e(t) \end{aligned} \tag{4}$$

where the current $i(t)$ and the voltage $v_l(t)$ are the input and output of the continuous-time linear sub-model model and the subscript l refers to linear. The output of the continuous-time linear sub-model $v_l(t)$ is the input of the output-static nonlinear function (nonlinear over-voltage function). The sigmoid function with an absolute expression is selected to describe the output static nonlinear function whose output is $v_W(t)$. The square-root expression adopted in [53] is replaced in this work, without loss of generality, by the absolute expression $v_l(t)$ for simplicity in forthcoming derivations. The constants c_1 and c_2 are real scalar weighting coefficients which signify the relative importance of the nonlinear function. The sampled form of $v_W(t)$ at instance k is denoted $v_W(t_k)$ where $t = kT_s$ and T_s is the sampling time. The last equation in (4) shows $v(t_k)$as the measured signal which is produced by corrupting the sum of $v_W(t_k)$and the open circuit voltage $v_{OCV}(t_k)$with discrete white (zero mean) noise $e(t_k)$representing the measurement noise. This process of including noise is usually known as output error, representing measurement noises. The continuous-time linear sub-model is described by input and output polynomials, denoted $B(\mathcal{D})$and $A(\mathcal{D})$,respectively, and are known, from Fig. 2 to be second order, such that:

$$\begin{aligned} A(\mathcal{D}) &= a_0\mathcal{D}^2 + a_1\mathcal{D} + a_2 \\ B(\mathcal{D}) &= b_0\mathcal{D}^2 + b_1\mathcal{D} + b_2 \end{aligned} \tag{5}$$

where $\mathcal{D}^n$ is the n^{th} order time derivative term d^n/dt^n, $n \in \mathbb{R}$ and the coefficients $a_j (j = 0,1,2)$ and $b_j (j = 0,1,2)$ are real and bounded to match the selected structure. The increase in order does not affect the derivation of the proposed algorithm.

4. Reformulation of the Wiener model for the WSRIVC method

This section illustrates how the nonlinear Wm presented in (4) can be re-arranged such that the relation between $i(t)$ and $v_W(t)$ is described by a linear model which then allows any linear estimator to be used in estimating the model parameters. Both $i(t)$ and $v_W(t)$ are assumed to be accessible and the parameter estimation is based on the collected $i(t)$ and $v_W(t)$ data. The second equation in (4) can be re-arranged and expressed as:

$$v_W(t) = c_1 v_l(t) - c_2 g(t) \tag{6}$$

where $g(t) = v_W(t)\|v_l(t)\|$. Replacing $v_l(t)$ with $\frac{B(\mathcal{D})}{A(\mathcal{D})} i(t)$ leads to a re-expression of (6) as:

$$v_W(t) = \frac{c_1 B(\mathcal{D})}{A(\mathcal{D})} i(t) - c_2 g(t) \tag{7}$$

It can readily be observed that c_1 and $B(\mathcal{D})$ can be combined without loss of generality. For simplicity c_1 is assumed to be a positive real constant. So this property can be used to reformulate (7) such that $\bar{B}(\mathcal{D}) = \bar{b}_0 s^2 + \bar{b}_1 s + \bar{b}_2$ and $\bar{g}(t) = v_W(t)\|\bar{v}_l(t)\|$ where $\bar{b}_i = c_1 b_i$ and $\bar{v}_l(t) = \frac{\bar{B}(\mathcal{D})}{A(\mathcal{D})}$. This leads to the re-expression of (7) as:

$$v_W(t) = \frac{\bar{B}(\mathcal{D})}{A(\mathcal{D})} i(t) - c\bar{g}(t) \tag{8}$$

where $c = c_2/c_1$.

5. SRIVC method for Wiener Sub-model (WSRIVC)

In what follows the *Wiener sub-model* is expressed within the framework of the simplified refined instrumental variable method for the continuous-time system identification. The Wm is re-expressed as a multi-input, single-output continuous-time model. Thus, the error function in (4), considering (8), can be expressed as:

$$\varepsilon_W(t) = v(t) - d_{OCV} - \left[\frac{\bar{B}(\mathcal{D})}{A(\mathcal{D})} i(t) - c\bar{g}(t)\right] \tag{9}$$

where the subscript W refers to Wiener and the offset d_{OCV} is a constant and is introduced to approximate the open circuit voltage within an infinitesimal SoC window. The Laplace transform of (9), considering zero initial conditions, is therefore:

$$E_W(s) = V(s) - d_{OCV}(s) - \left[\frac{\bar{B}(s)}{A(s)} I(s) - c\bar{G}(s)\right] \tag{10}$$

where $d_{OCV}(s) = \frac{1}{s} d_{OCV}$ and the Laplace transforms of the output and input polynomials, respectively, are given by:

$$\begin{aligned} A(s) &= a_0 s^2 + a_1 s + a_2 \\ \bar{B}(s) &= \bar{b}_0 s^2 + \bar{b}_1 s + \bar{b}_2 \end{aligned} \tag{11}$$

To approximate the derivative terms, while retaining $E_W(s)$ on the left-hand side of (10) without filtering, a filter $\frac{1}{A(s)}$ is introduced in the first term on the right hand side of (10). This step leads to the

introduction of an output polynomial $A(s)$ in the first term of (10) as follows:

$$E_W(s) = A(s)\frac{1}{A(s)}V(s) - d_{OCV}(s) - [\bar{B}(s)\frac{1}{A(s)}I(s) - c\bar{G}(s)] \quad (12)$$

Eq. (12) can then be transformed back to the time-domain and expressed as:

$$\varepsilon_W(t) = A(\mathcal{D})\frac{1}{A(\mathcal{D})}v(t) - d_{OCV} - [\bar{B}(\mathcal{D})\frac{1}{A(\mathcal{D})}i(t) - c\bar{g}(t)] \quad (13)$$

It can be observed that $\bar{g}(t)$ is not filtered by $\frac{1}{A(\mathcal{D})}$.This is because the function $\bar{g}(t)$ does not contain derivative terms which is required for estimation. Thus, the error function in (13) is rearranged and described in a filtered form as:

$$\varepsilon_W(t) = A(\mathcal{D})v_F(t) - d_{OCV} - [\bar{B}(\mathcal{D})i_F(t) - c\bar{g}(t)] \quad (14)$$

where the subscript F denotes a signal filtered by $\frac{1}{A(\mathcal{D})}$. The filtered input and output are $i_F(t)$ and $v_F(t)$, respectively, and are obtained by:

$$\begin{aligned} i_F(t) &= \tfrac{1}{A(\mathcal{D})}i(t) \\ v_F(t) &= \tfrac{1}{A(\mathcal{D})}v(t) \end{aligned} \quad (15)$$

The pseudo-linear regression form can be obtained from the sampled form of (15) and expressed as:

$$\mathcal{D}^2 v_F(t_k) = \varphi_{F,W}^T(t_k)\theta_W + \varepsilon_w(t_k) \quad (16)$$

where $a_0 = 1$ and

$$\theta_W = [\,a_1, \quad a_2, \quad \bar{b}_0, \quad \bar{b}_1, \quad \bar{b}_2, \quad c, \quad d_{OCV}\,]^T \quad (17)$$

$$\varphi_{F,W}^T(t_k) = [\,-\mathcal{D}v_F(t_k), \; -v_F(t_k), \; \mathcal{D}^2 i_F(t_k), \; \mathcal{D}i_F(t_k), \; i_F(t_k), \; -\bar{g}(t_k), \; 1\,] \quad (18)$$

The $\bar{g}(t_k)$ function is not directly accessible. However, since $\bar{g}(t_k)$ is a function of $v_l(t_k)$ and $v_W(t_k)$, it can be simulated based on previously (recent) obtained estimates. The estimated $\hat{v}_l(t_k)$ and $\hat{v}_W(t_k)$ can be approximated using $\hat{c}$, $\hat{d}_{OCV}$, $\hat{v}_l(t_k)$, $\hat{\bar{B}}(\mathcal{D})$ and $\hat{A}(\mathcal{D})$. In this paper, the first $\hat{\bar{B}}(\mathcal{D},\hat{\theta}_{1,W})$ and $\hat{A}(\mathcal{D},\hat{\theta}_{1,W})$ polynomials are selected with the following considerations: (i) the output steady state of the linear system, (ii) the type of linear system, whether it is under-damped or over-damped, and (iii) the cut-off frequency that can be selected according to the state variable filter design [67]. Similarly, the initial filter in (15) can be selected as $\frac{1}{\hat{A}(\mathcal{D},\hat{\theta}_{1,W})}$. The nonlinear and offset coefficients $\hat{c}$ and $\hat{d}_{OCV}$ are selected to be zeros.

The iterative WSRIVC method is illustrated in Fig. 3 and its execution is summarised as follows:

Simulate the noise-free output $\hat{\bar{v}}_l(t)$ using:

$$\hat{\bar{v}}_l(t) = \frac{\hat{\bar{B}}(\mathcal{D},\hat{\theta}_{L-1,W})}{\hat{A}(\mathcal{D},\hat{\theta}_{L-1,W})}i(t_k) \quad (19)$$

$$\hat{v}_W(t) = \frac{\hat{\bar{v}}_l(t)}{1 + \hat{c}\|\hat{\bar{v}}_l(t)\|} \quad (20)$$

where $\hat{\bar{v}}_l(t)$ and $\hat{v}_W(t)$ are used as the input to $\hat{\bar{g}}_i(t_k)$. The subscript L indicates the current iteration number and $L-1$ indicates the previous iteration number.

Filter $v(t_k)$ and $i(t_k)$ to generate their respective filtered forms containing higher derivatives, using:

$$F(D) = \frac{1}{\hat{A}(\mathcal{D},\hat{\theta}_{L-1,W})} \quad (21)$$

Generate $\hat{\bar{g}}(t_k)$ in (18) using $\hat{\bar{v}}_l(t)$ and $\hat{v}_W(t)$.

Obtain the estimated parameters using the LS algorithm:

$$\hat{\theta}_{l,W} = \Big(\sum_{k=1}^{N}\hat{\varphi}_{F,W}(t_k)\hat{\varphi}_{F,W}^T(t_k)\Big)^{-1}\sum_{k=1}^{N}\hat{\varphi}_{F,W}(t_k)\mathcal{D}^2 v_F(t_k) \quad (22)$$

where $\hat{\varphi}_{F,W}^T$ is defined as:

$$\hat{\varphi}_{F,W}^T(t_k) = [\,-\mathcal{D}v_F(t_k), \; -v_F(t_k), \; \mathcal{D}^2 v_{l,F}(t_k), \; \mathcal{D}v_{l,F}(t_k), \; v_{l,F}(t_k), \; -\hat{\bar{g}}(t_k), \; 1\,] \quad (23)$$

There is no need to use the instrumental variable regression vector because the estimated $\bar{g}(t_k)$ is used as an instrumental variable.

Iterate from (I) to (IV) until the sum of the squares of the differences between $\hat{\theta}_{L-1,W}$ and $\hat{\theta}_{L,W}$ is significantly small $\|\hat{\theta}_{L-1,W} - \hat{\theta}_{L,W}\| < 10^4$ or for a defined number of iterations. The maximum number of iterations is selected to be 5 such that the steps (I)

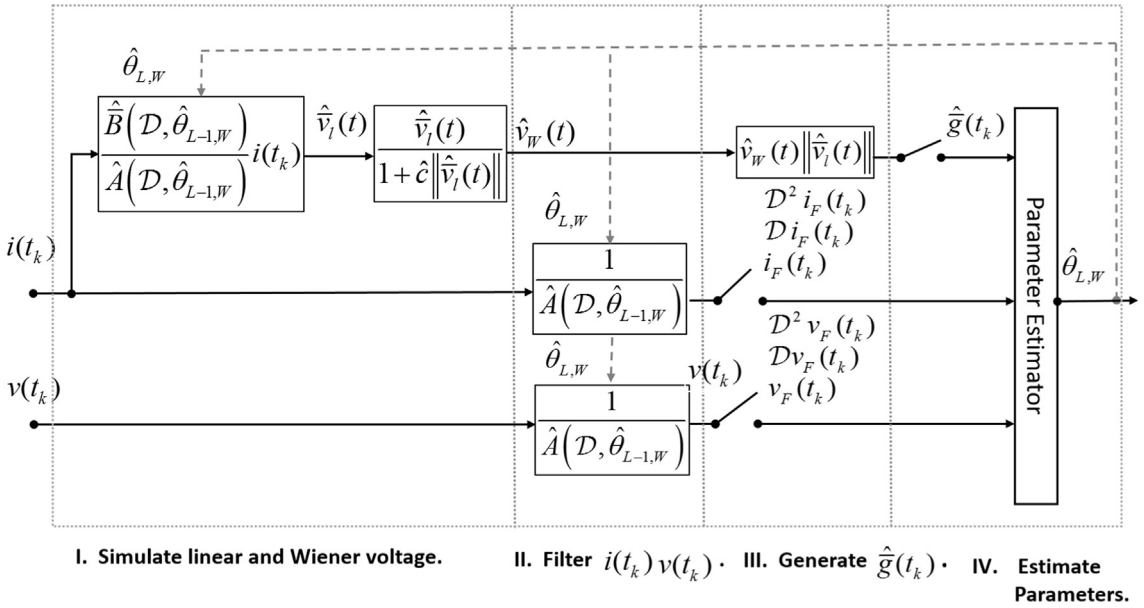

Fig. 3. The block diagram of the WSRIVC approach shows steps I to IV.

to (IV) are repeated until $L = 5$. This is because in a case study presented later, convergence is found to occur after 3 iterations.

6. On-line parameter estimation and updating

This section presents how the off-line estimation can be extended to on-line estimation. Since the parameters can be estimated off-line and the model can be expressed in linear regression form, as given in (16), the off-line estimator can be extended to on-line estimation. This estimation process is divided into linear and nonlinear parts where the linear estimation extracts the parameters of the linear submodule and the nonlinear estimation part obtains the nonlinear coefficients.

For estimating the linear sub-model parameters, there is a need to estimate the linear voltage $\hat{\bar{v}}_l(t_k)$, given in (20) and illustrated in Fig. 1. The linear voltage can be estimated using the inverse of the $v_w(t_k)$ function in (20) which is expressed as:

$$\hat{\bar{v}}_l(t_k) = \frac{\hat{v}_W(t_k)}{1 - \hat{c}(t_k)\|\hat{v}_W(t_k)\|} \tag{24}$$

where $\hat{v}_W(t_k) = v(t_k) - \hat{d}_{OCV}(t_k)$. Since the input $\hat{\bar{v}}_l(t_k)$ and output $v(t_k)$ of the linear sub-model are realisable, the pseudo- regression form of the linear sub-model can be derived and expressed as:

$$\mathcal{D}^2\bar{v}_{F,l}(t_k) = \varphi^T_{F,l}(t_k)\theta_l \tag{25}$$

where $a_0 = 1$ and

$$\theta_l = [\,a_1, \quad a_2, \quad \bar{b}_0, \quad \bar{b}_1, \quad \bar{b}_2\,]^T \tag{26}$$

$$\varphi^T_{F,l}(t_k) = [\,-\mathcal{D}\bar{v}_{F,l}(t_k), \quad -\bar{v}_{F,l}(t_k), \quad \mathcal{D}^2 i_F(t_k), \quad \mathcal{D}i_F(t_k), \quad i_F(t_k)\,] \tag{27}$$

Following the classical derivation of the RLS algorithm with an inherent mechanism for tracking time-varying parameters as given in [68], the general form of RLS is expressed as:

Prediction Step:

$$\begin{aligned} \hat{\theta}_l(t_k) &= \hat{\theta}_l(t_{k-1}) \\ P^*(t_k) &= P^*(t_{k-1}) + \textstyle\sum_v \end{aligned} \tag{28}$$

Correction Step:

$$\begin{aligned} L(t_k) &= P^*(t_k)\hat{\varphi}_{F,l}(t_k)(1 + \hat{\varphi}^T_{F,l}(t_k)P^*(t_k)\hat{\varphi}_{F,l}(t_k))^{-1} \\ \hat{\theta}_l(t_k) &= \hat{\theta}_l(t_k) + L(t_k)(\mathcal{D}^2\bar{v}_{F,l}(t_k) - \hat{\varphi}^T_{F,l}(t_k)\hat{\theta}_l(t_{k-1})) \\ P^*(t_k) &= (P^*(t_k) - L(t_k)\hat{\varphi}^T_{F,l}(t_k)P^*(t_{k-1})) \end{aligned} \tag{29}$$

The initial values of $P^*(0)$ are selected as $P^*(0) = \mu I$ where $\mu > 0$ and I is an identity matrix while $\sum_v = \lambda I$ and $0 < \lambda < 1$. In this paper, they are selected such as $\lambda = 10^{-6}$ and $P(0) = 10^{-4} \times I$. This is because $\theta_n(0)$ is extracted from θ_W which is obtained from the off-line estimation. This means there is no need for large corrections.

The sampling interval of the nonlinear estimation (T_K) is 250 times slower than the linear estimation sampling interval $T_K = 250T_k$ where T_k is the sampling time of the system and is selected to be $T_k = 0.1s$ for linear estimation. The form for the pseudo-linear regression, considering that the nonlinear parameters are derived from the substitution of Eq. (8) into the last equation in (4), can be expressed as:

$$x(t_K) = \varphi^T_n(t_K)\theta_n \tag{30}$$

where

$$x(t_K) = v(t_K) - \bar{v}_l(t_K) \tag{31}$$

$$\theta_n = [\,c, \quad d_{OCV}\,]^T \tag{32}$$

$$\varphi^T_n(t_K) = [\,-\bar{g}(t_K), \quad 1\,] \tag{33}$$

The parameter vector θ_n at sample K is obtained using all data collected between $K-1$ and K in the LS algorithm by using:

$$\hat{\theta}_n(t_K) = \Big(\sum_{k=K-1}^{K}\varphi_n(t_k)\varphi^T_n(t_k)\Big)^{-1}\sum_{k=K-1}^{K}\varphi_n(t_k)x(t_k) \tag{34}$$

The iterative on-line estimation process is illustrated in Fig. 4 and summarised as follows:

I. Use the estimated nonlinear parameters vector $\hat{\theta}_n(t_{K-1}) = [\hat{c}\hat{d}_{OCV}]$ for estimating $\hat{v}_l(t_k)$ using the inverse function in (24) where $\hat{\theta}_n(0)$ is obtained using off-line estimation.
II. Filter $\hat{v}_l(t_k)$ and $i(t_k)$ for producing their filtered data using:

$$F(D) = \frac{1}{\hat{A}(\mathcal{D}, \hat{\theta}_{L-1,l}(t_{k-1}))} \tag{35}$$

III. Obtain the estimated parameters $\hat{\theta}_l(t_k)$ using RLS given in (28) where subscript L refers to the iteration number.
IV. Update the parameters in the NL-ECM at the sample k.
V. Steps I to IV are repeated for $L = 3$ iterations.
VI. Update $\hat{\theta}_n(t_{K-1})$ at $t = t_K$. Updating $\hat{\theta}_n(t_{K-1})$ is achieved by the following steps:
   i. Use the matrix of parameter vectors $\hat{\theta}_l(t_{k:K})$ and $\hat{c}(t_{K-1})$ to simulate $\hat{\bar{v}}_l(t)$ using:

$$\hat{\bar{v}}_l(t_{k:K}) = \frac{\hat{\bar{B}}(\mathcal{D}, \hat{\theta}_l(t_{k:K}))}{\hat{A}(\mathcal{D}, \hat{\theta}_l(t_{k:K}))}i(t_{k:K}) \tag{36}$$

$$\hat{v}_W(t_{k:K}) = \frac{\hat{\bar{v}}_l(t_{k:K})}{1 + \hat{c}(t_{K-1})\|\hat{\bar{v}}_l(t_{k:K})\|} \tag{37}$$

   where vectors $\hat{\bar{v}}_l(t_{k:K})$ and $\hat{v}_W(t_{k:K})$ are used as inputs to generate $\hat{\bar{g}}_i(t_{k:K})$
   ii. Obtain the estimated parameters using (34).
   iii. Use $\hat{\theta}_n(t_K)$ to update the nonlinear parameters in the NL-ECM and return to step I for the next sample.

7. Results and discussion

The results obtained from the approach proposed in this paper, in terms of estimation efficiency (off-line convergence and on-line parameter estimation) and physical parameters (i.e., $R_0, R_{P1}, R_{P2}, \tau_{P1}, \tau_{P2}, d_{OCV}, c$), are presented in this section.

The algorithm was tested with experimental data collected from a commercial 3Ah 18650-type cell which comprises graphite negative electrode, a $LiNiCoAlO_2$ positive electrode and commercial electrolyte. For off-line parameter estimation, data was collected at 20 different battery operating points which are the various combinations of SoC $= [10\%, 20\%, 50\%, 80\%, 95\%]$ and temperatures $T = [0^oC, 10^oC, 25^oC, 45^oC]$. At each operating point, a

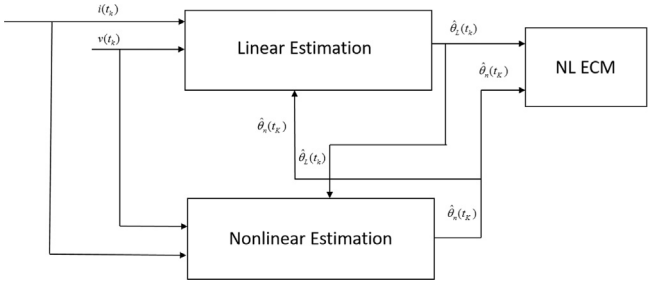

Fig. 4. On-line estimation block diagram of NL-ECM.

pulse-multisine current signal [53] is applied to the cell using a Bitrode cell cycler. The corresponding voltage response is measured. An example, of the pulse-multisine current signal and the voltage response for the 3 Ah 18650 cell used in this work is shown in Fig. 5. Within the figure, a positive current indicates charging while a negative current depicts discharge. For increased robustness of results, four different cells were tested. Thus, the algorithm was executed, off-line, 80 times.

The estimated parameters are averaged over four cells. Because the parameters are state-dependent (i.e., dependant on SoC and temperature), the obtained parameters for a given state are put into a 2D look-up table and are linearly interpolated to approximate the parameters between the selected intervals.

7.1. Off-line estimator performance

The convergence of the algorithm is typically determined by the stability of the linear sub-model of the NL-ECM. The estimations of the linear sub-model obtained in all-20 iterations, for 80 runs, were found to be numerically stable. To facilitate the discussion, the results of one run – corresponding to $T = 0^0C$ and $SoC = 95\%$ – is addressed in this subsection. This particular combination was chosen because at low temperatures and extreme SoC values the battery is known to exhibit strong nonlinear characteristics. Fig. 6 shows that the estimates converge to acceptable values in the third iteration. The results also show that after the third iteration, there is no significant difference in magnitude and phase. It can also be noted that for higher frequencies (circa. $\omega > 2rad \cdot s^{-1}$), both phase and magnitude do not fluctuate around one value but both increase as the iteration number increases. This may be because the system is of much higher order.

The convergence of the coefficient of the nonlinear overpotential function c is given in Table 1. The offset parameter d_{OCV} stabilised in the second iteration and negligibly changed as the number of iterations increased beyond 2, as shown in Fig. 7. The performance of the estimated nonlinear overpotential function is shown in Fig. 8. It can be seen that, apart from the first iteration which is the initial value, the performance exhibits no difference after the second iteration. These results highlight the efficiency of the estimator performance and convergence. Although the WSRIVC is modified for the nonlinear model shown in Fig. 1, it provides similar statistical convergence of parameters, as shown in Table 1, and frequency response, as shown in Fig. 6, to results obtained using the SRIVC method [69] which was designed for the linear system. This efficiency in convergence and frequency response mean that the proposed method can be applied online to estimate the parameters of nonlinear models with the same computational effort as traditional linear models. More investigation however, is required to fully understand the higher frequency performance of the model. For this purpose, the ECM defined in Fig. 2, which is inherently limited by the bandwidth, needs to be reformulated to capture a higher frequency range, using for example, constant phase element blocks.

7.2. Identified model parameters

The proposed algorithm in this paper is used to estimate the NL-ECM parameters for a 3 Ah C_6/$LNiCoAlO_2$ 18650 Li-ion battery using a pre-defined set of pulse-multisine signals. The mean and standard deviation of the NL-ECM parameters $R_0,\ R_{p1},\ R_{p2}\,\tau_{p1},\ \tau_{p2}, c\ \ d_{OCV}$, calculated over four cells, corresponding to each battery state, are tabulated in Table 1. It is note-

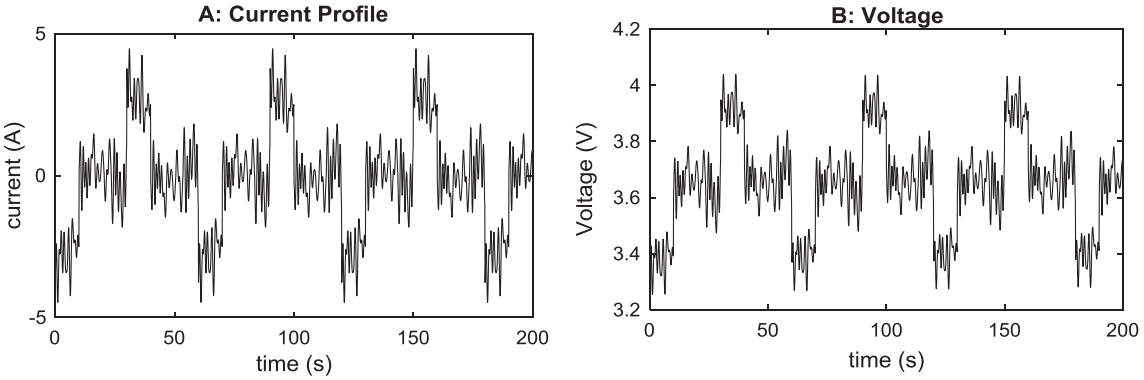

Fig. 5. Pulse-multisine test at SoC = 50% and $T = 0^oC$. (A) The current and (B) the voltage response.

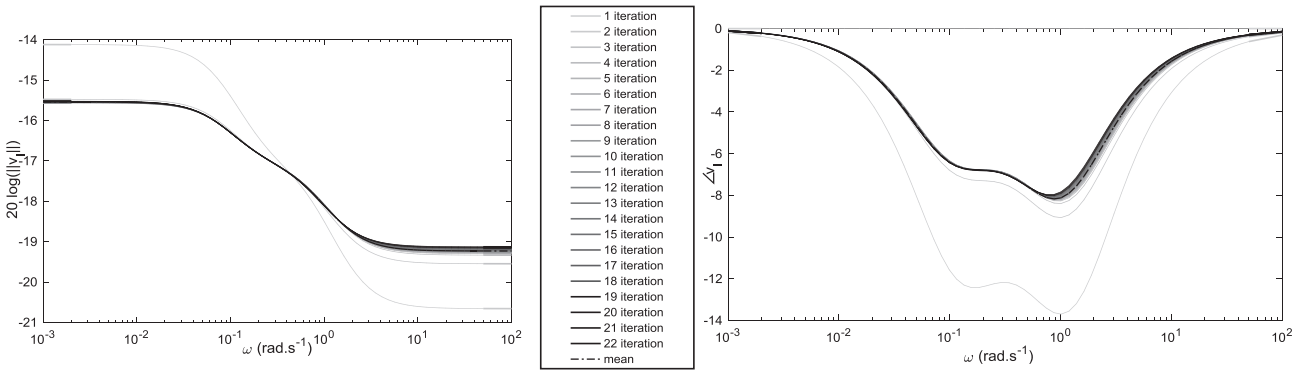

Fig. 6. Shows the logarithmic magnitude of y_1 (left panel) and the phase (right panel) against frequency response of the linear sub-model for 20 iterations obtained using the off-line WSRIVC method. The first iteration is depicted in lightest grey-line, the last iteration is presented in black-line; consecutively darker shades of grey are used for larger iteration numbers. The mean of the last ten iterations is depicted by a black-dashed-line. The multisine test data at $T = 0^0C$ and SoC = 95% are used here.

Table 1
The mean and standard deviation of the estimated ECM and nonlinear over-voltage function coefficient of the NL-ECM model based on the four 18650 3.03 Ah Li-ion NCA cells, using the multisine test data at 20 different SoC and temperature combinations.

Temp	SoC	R_0 (mΩ)	R_{p1} (mΩ)	R_{p2} (mΩ)	τ_{p1} (s)	τ_{p2} (s)	c	d_{OCV}
0 °C	10%	97.5 ± 1.7	82.5 ± 0.8	9.2 ± 0.465	1.1 ± 0.009	10.1 ± 0.12	$0.0549 \pm 5 \times 10^{-4}$	$3.4 \pm 3 \times 10^{-3}$
	20%	91.3 ± 1	73.4 ± 2.2	1.8 ± 0.075	0.9 ± 0.003	12.2 ± 0.13	$0.0356 \pm 9 \times 10^{-4}$	$3.5 \pm 3.4 \times 10^{-3}$
	50%	82.5 ± 1.2	10.1 ± 0.4	1.4 ± 0.004	0.9 ± 0.005	11.2 ± 0.08	$0.0087 \pm 1 \times 10^{-4}$	$3.7 \pm 0.7 \times 10^{-3}$
	80%	74.4 ± 1	8.1 ± 0.2	1.6 ± 0.004	0.9 ± 0.003	15.4 ± 0.1	$-0.0015 \pm 3 \times 10^{-4}$	$3.8 \pm 2.1 \times 10^{-3}$
	95%	111.3 ± 1.8	25.3 ± 0.4	2.6 ± 0.038	1.2 ± 0.010	10.7 ± 0.06	$-0.047 \pm 14 \times 10^{-4}$	$4.0 \pm 1.5 \times 10^{-3}$
10 °C	10%	92.9 ± 1.8	23.8 ± 1.4	6.7 ± 0.444	1.3 ± 0.049	10.5 ± 0.09	$0.085 \pm 7 \times 10^{-4}$.3	$3.3 \pm 7 \times 10^{-3}$
	20%	68.1 ± 0.9	18.9 ± 0.9	1.3 ± 0.017	0.8 ± 0.005	11.9 ± 0.09	$0.022 \pm 7 \times 10^{-4}$	$3.5 \pm 1.1 \times 10^{-3}$
	50%	52.6 ± 0.6	0.9 ± 0	0.2 ± 0.003	0.9 ± 0.001	12.9 ± 0.06	$0.003 \pm 1 \times 10^{-4}$	$3.6 \pm 1.1 \times 10^{-3}$
	80%	56.8 ± 0.8	1.7 ± 0.1	1.5 ± 0.006	1.0 ± 0.004	12 ± 0.05	$0.003 \pm 3 \times 10^{-4}$	$3.9 \pm 1.2 \times 10^{-3}$
	95%	70.5 ± 1	7.4 ± 0.2	8.8 ± 0.009	0.9 ± 0.003	11.9 ± 0.07	$-0.0087 \pm 6 \times 10^{-4}$	$4.1 \pm 0.7 \times 10^{-3}$
25 °C	10%	53.2 ± 0.5	27 ± 1	1.9 ± 0.058	0.7 ± 0.001	12.5 ± 0.09	$0.06 \pm 15 \times 10^{-4}$	$3.4 \pm 3.6 \times 10^{-3}$
	20%	45.4 ± 0.5	1.9 ± 0.1	1.1 ± 0.003	0.8 ± 0.005	12.8 ± 0.11	$0.014 \pm 4 \times 10^{-4}$	$3.5 \pm 1.4 \times 10^{-3}$
	50%	36.4 ± 0.5	0.1 ± 0.1	0.8 ± 0.005	0.8 ± 0.002	14.1 ± 0.07	$0.006 \pm 1 \times 10^{-4}$	$3.6 \pm 1.0 \times 10^{-3}$
	80%	37.4 ± 0.5	0.5 ± 0	0.9 ± 0.005	0.9 ± 0.002	12.9 ± 0.08	0.0087 ± 1.3	$3.9 \pm 2.1 \times 10^{-3}$
	95%	50.5 ± 0.8	0.5 ± 1.3	1.5 ± 0.016	0.9 ± 0.004	10.5 ± 0.06	$0.0078 \pm 7 \times 10^{-4}$	$4.1 \pm 0.6 \times 10^{-3}$
45 °C	10%	33.7 ± 0.4	1.9 ± 0.1	0.9 ± 0.002	0.8 ± 0.005	12.6 ± 0.05	$0.016 \pm 6 \times 10^{-4}$	$3.4 \pm 2.3 \times 10^{-3}$
	20%	30.4 ± 0.4	0.6 ± 0	0.8 ± 0.004	0.8 ± 0.004	11.5 ± 0.06	$0.005 \pm 1 \times 10^{-4}$	$3.5 \pm 1.3 \times 10^{-3}$
	50%	27.7 ± 0.4	0.68 ± 0.1	0.6 ± 0.008	0.8 ± 0.003	12.7 ± 0.05	$0.0089 \pm 2 \times 10^{-4}$	$3.7 \pm 1.4 \times 10^{-3}$
	80%	27.6 ± 0.4	0.4 ± 0	0.8 ± 0.004	0.9 ± 0.003	13.1 ± 0.06	$0.0169 \pm 2 \times 10^{-4}$	$3.9 \pm 1.4 \times 10^{-3}$
	95%	31.1 ± 0.5	0.0243 ± 0.1	1 ± 0.006	0.9 ± 0.001	11.2 ± 0.05	$0.0117 \pm 5 \times 10^{-4}$	$4.1 \pm 1.1 \times 10^{-3}$

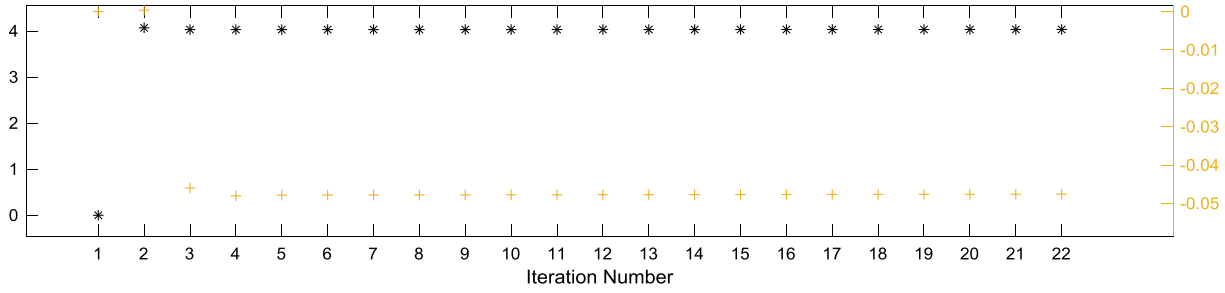

Fig. 7. The estimated c and d_{OCV} for 22 iterations.

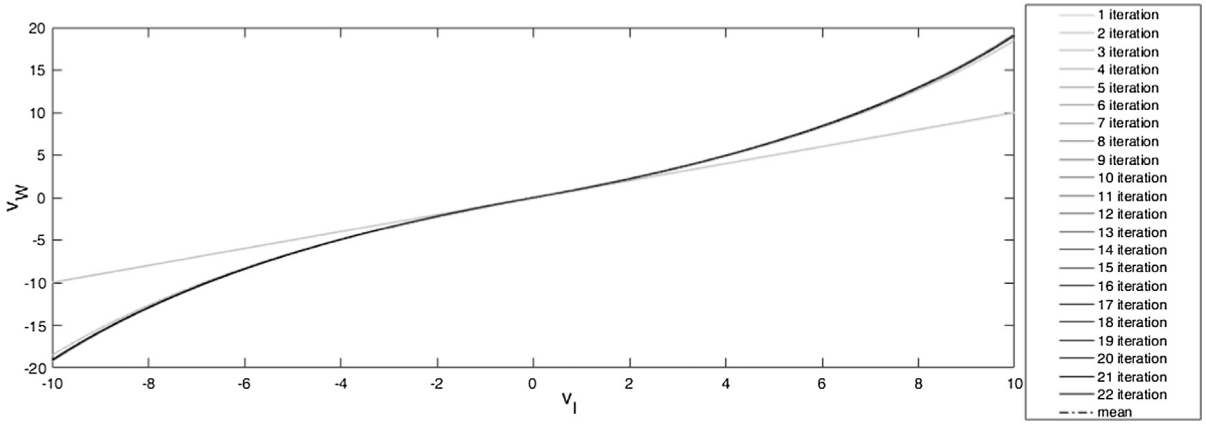

Fig. 8. Estimated nonlinear over-potential function. The multisine test data at $T = 0^0C$ and $SoC = 95\%$ are used here.

worthy to highlight that the trend of R_o in Table 1 varies with SoC, contrary to what is expected by definition [3]. As previously discussed in Section 2, theoretically, R_o is the pure Ohmic resistance of the battery corresponding to a frequency $f \gg 1Hz$, while R_{p1} and R_{p2} are associated with the charge-transfer process ($f \geqslant 1$ Hz) and ionic diffusion (10^{-3} Hz $\leqslant f \leqslant 1$ Hz), respectively. A major drawback of the Multisine approach, adopted in this work due to its suitability for online parameter estimation, is that R_o is no longer well defined. The principal component of the driving multisine current load is $f = 1$ Hz. Thus, the analogy of the ECM components with physio-chemical sub-processes are undermined. This issue is also persistent in pulse power experiments (typically $f \leqslant 0.1$ Hz). Nevertheless, the sum of resistances R_0, R_{p1}, R_{p2}, which will govern the voltage response, at all temperatures follow the general theoretical trend for cell resistance as a function of SoC. That is, the total resistance is at a minimum for circa. 50% SoC, with the highest resistances observed as SoC tends towards 0% and 100% SoC (although total resistance is higher for 0% than

100% SoC) as shown in the leftmost plot in Fig. 9. Moreover, the leftmost plot in Fig. 9 illustrates that the increase in temperature causes a reduction in all resistance parameters.

Nonlinearity, quantified by c, is found to be most significant at low SoCs and low temperatures, where ion dynamics are relatively slower. For higher values of SoC and temperatures, c is found to be small, such that $v_w = \frac{\bar{v}_l}{1+c\|\bar{v}_l\|} \approx \bar{v}_l$. That is, in the $c \ll 1$, the shape of the sigmoid is incentive to c.

As expected, the estimated offset parameter $\hat{d}_{OCV}$ is highly correlated to the SoC such that a higher offset is obtained with higher SoC, as shown in Table 1 and the rightmost plot in Fig. 9. The temperature has an insignificant effect on the estimated offset parameter, in agreement with previous studies [63].

Using the estimated mean parameters presented in Table 1, the NL-ECM model is validated with a charge sustaining drive-cycle current profile recorded from a prototype EV when driving in an urban environment with frequent acceleration and regenerative braking events. This highly dynamic driving cycle is employed for validation because under extended periods of high current loads, the battery enters a regime of diffusion limitation [52] where the NL extension to the linear ECM becomes significant. Such a current profile was also used for validation in [53] where the first order linear ECM displayed a root-mean-square error of 3.3×10^{-2} under the same SoC and temperature conditions considered in this work. As shown in Fig. 10, there is very good agreement between the measured and modelled voltage. The proposed model generates a root-mean-square error of 2.51×10^{2} over 1200 s of cycling, which represents a significant improvement from the linear case [53,63].

7.3. On-line estimation

The result of on-line estimation is presented in Fig. 11. The results for on-line estimation show a more accurate voltage estimation than its off-line counterpart, which is clearly identified by comparing the voltage error in Figs. 10(B)–11(B). It is noteworthy that in the first 200 s a large correction occurred following which all the estimates tend to an asymptotic value. The model parameters are also shown to smoothly converge, as illustrated in Fig. 11(C–J). The accuracy of the estimates of the linear sub-model leads to an almost zero error for approximately three-quarters of the 1200 s load cycle. This was because the iterative technique used for the on-line estimation of parameters sampled at each time step, thus improving the correction. The excessive, but inexpensive, corrections to the parameter estimates caused a minimisation of the error between the modelled and actual voltages.

Because the error between the modelled and actual voltages is zero after the first circa. 200 s, the nonlinear coefficient was not subject to significant corrections, as shown in Fig. 11(J). This is

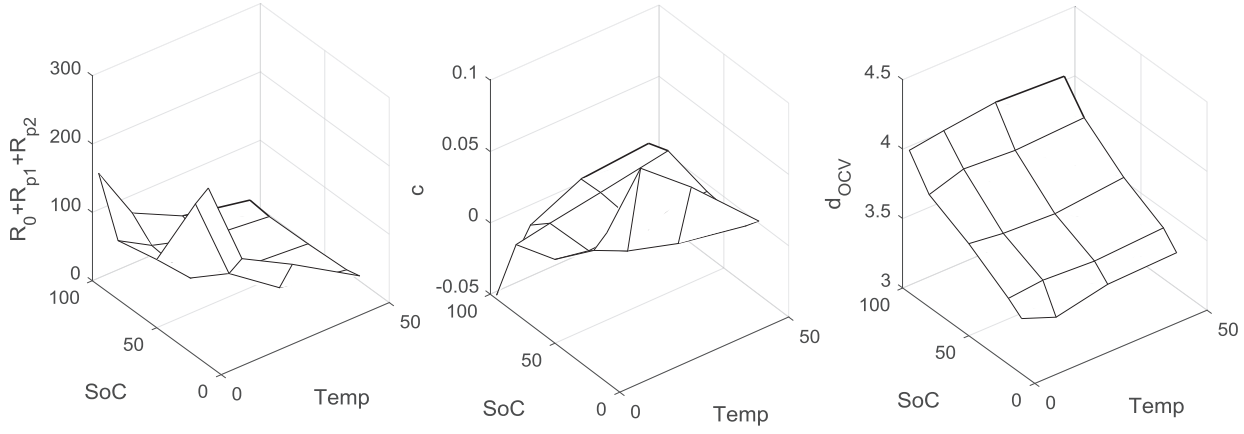

Fig. 9. Sum of the resistance elements in the NL-ECM is presented on the left-side, the estimated nonlinear coefficient $\hat{c}$ is located on the middle and $\hat{d}_{OCV}$ plot is on the right-side.

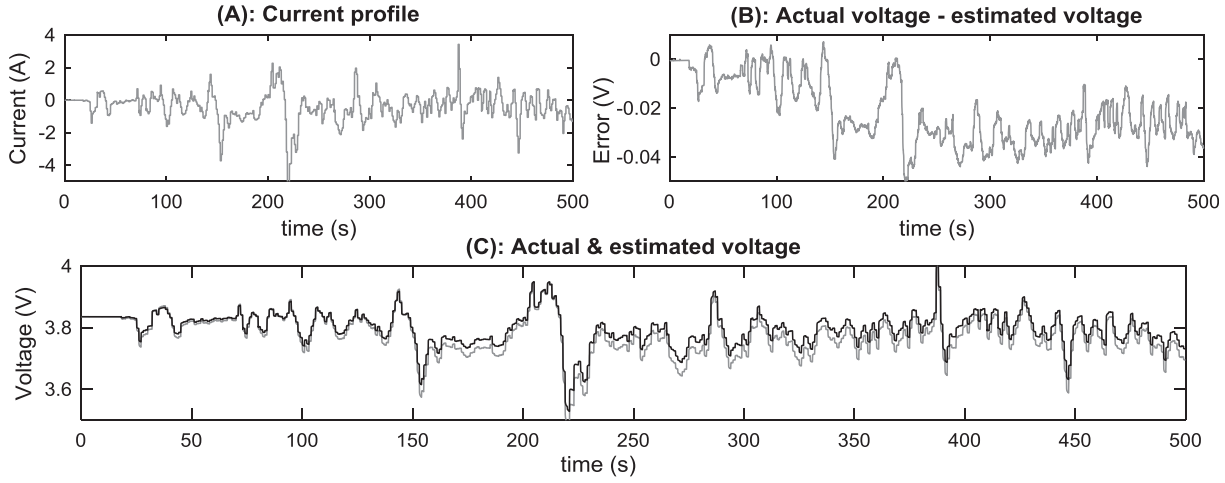

Fig. 10. Validation results of current drive cycle for first 500 s of the 1200 s at 70% SoC and temperature at 10 °C in (A) and the difference between measured and modelled voltage in (B) and measured and model voltage in (C) and presented in black and grey, respectively.

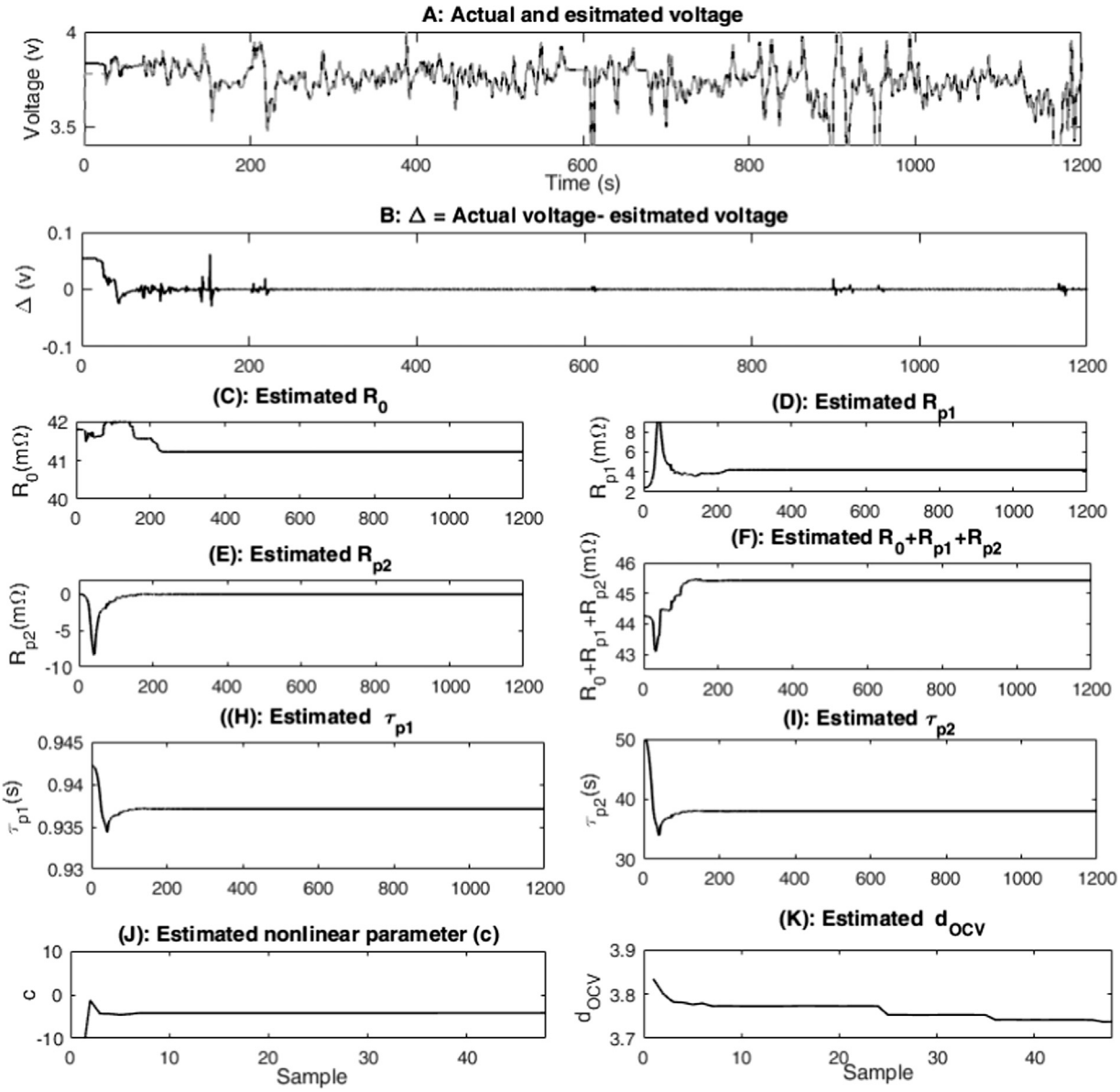

Fig. 11. The results of on-line estimation and prediction of NL-ECM with the same validation profile, shown in Fig. 10 where (A) shows the predicted and actual voltages, (B) gives the error between the actual and estimated voltages (C–F) present the resistance in the NL-ECM in a form of R_0, R_{p1} R_{p2} and $R_0 + R_{p1} + R_{p2}$, respectively, (G, H) are the time constants τ_{p1} and τ_{p2}, respectively and (I, J) show the estimated nonlinear coefficient c and offset d_{OCV}, respectively, for 48 samples because estimation of the nonlinear part occurs after 25 s. The test is run at 70% SoC and temperature at 10 °C.

because the correction factor is a function of error. The charge sustaining drive cycle used to demonstrate on-line parameter estimation consumed a total of 6% SoC (from a starting SoC of 70%). For the commercial battery considered in this study, this change in SoC corresponds to an OCV change of more than 70 mV.

8. Conclusions and further work

8.1. Conclusions

In this paper, a novel algorithm is proposed that directly estimates the model parameters of a nonlinear equivalent circuit model from observed input–output data. The parameter estimation algorithm extends the simplified refined instrumental variable method to estimate the Wiener model, which itself was reformulated into a multi-input/single-output linear model using a static nonlinear function (i.e., sigmoid function) that characterises the nonlinear voltage response of a LIB under a diffusion limited regime. A recursive least squares algorithm was then employed for parameter estimation.

The iterative offline estimation algorithm is extended to an iterative online estimation. The online estimation is divided into two sub-estimators. The first estimator extracts the parameters of the linear sub-model and executes at timescales within the sampling timescale of collected data. The second sub-estimator obtains the coefficient of the nonlinear static function and the offset and runs after a pre-defined number of samples.

Both on-line and off-line approaches were applied to a commercially available 3Ah C_6/$LNiCoAlO_2$ 18650-type cell using pulse-multisine tests. The extracted parameters were then validated using a charge sustaining drive-cycle recorded from a prototype electric vehicle driving in an urban environment. Both the on-line and off-line validation results showed very good agreement with measured terminal voltage. The parameter estimation

algorithm for the nonlinear battery model proposed in this work exhibited fast convergence, similar to that demonstrated with linear models [69], which is advantageous for on-line BMS applications. In addition, the algorithm depends only on the on-board available signals, i.e., the battery terminal voltage and current measurements, and thus is suitable for EV applications. The low model complexity and the efficient recursive algorithm can facilitate real time implementation.

8.2. Further work

The model was validated using short-term drive cycle data, so it is difficult to assess how the model will adapt to changes in battery characteristics due to the aging process. Future work will thus focus on state of health estimation, in particular assessing the algorithm response to battery degradation. In addition to SoH, it will also be of interest to investigate the possibility of using this, more accurate identification procedure, for OCV estimation and hence online SoC estimation.

Acknowledgements

This research was supported by the Engineering and Physical Science Research Council grants EP/M507143/1, EP/N001745/1 and EP/P511432/1.

References

[1] Wang Y, Chen Z, Zhang C. On-line remaining energy prediction: a case study in embedded battery management system. Appl Energy 2017;194:688–95.
[2] Marongiu A, Nußbaum FGW, Waag W, Garmendia M, Sauer DU. Comprehensive study of the influence of aging on the hysteresis behavior of a lithium iron phosphate cathode-based lithium ion battery – an experimental investigation of the hysteresis. Appl Energy 2016;171:629–45.
[3] Waag W, Käbitz S, Sauer DU. Experimental investigation of the lithium-ion battery impedance characteristic at various conditions and aging states and its influence on the application. Appl Energy 2013;102(Feb):885–97.
[4] Vetter J, Novák P, Wagner MR, Veit C, Möller K-C, Besenhard JO, Winter M, Wohlfahrt-Mehrens M, Vogler C, Hammouche A. Ageing mechanisms in lithium-ion batteries. J Power Sources 2005;147(1):269–81.
[5] K. Uddin, S. Perera, W. Widanage, L. Somerville, J. Marco, Characterising lithium-ion battery degradation through the identification and tracking of electrochemical battery model parameters, Batteries, vol. 2, no. 2. Multidisciplinary Digital Publishing Institute, p. 13, Apr-2016.
[6] Uddin K, Moore AD, Barai A, Marco J. The effects of high frequency current ripple on electric vehicle battery performance. Appl Energy 2016;178:142–54.
[7] Uddin K, Somerville L, Barai A, Lain M, Ashwin TR, Jennings P, Marco J. The impact of high-frequency-high-current perturbations on film formation at the negative electrode-electrolyte interface. Electrochim Acta 2017.
[8] Cannarella J, Arnold CB. State of health and charge measurements in lithium-ion batteries using mechanical stress. J Power Sources 2014;269:7–14.
[9] Xing Y, Ma EWM, Tsui KL, Pecht M. Battery management systems in electric and hybrid vehicles. Energies 2011;4(12):1840–57.
[10] Lu L, Han X, Li J, Hua J, Ouyang M. A review on the key issues for lithium-ion battery management in electric vehicles. J Power Sources 2013;226:272–88.
[11] Zhang J, Lee J. A review on prognostics and health monitoring of Li-ion battery. J Power Sources 2011;196(15):6007–14.
[12] Pop V, Bergveld HJ, Notten PHL, Regtien PPL. State-of-the-art of battery state-of-charge determination. Meas Sci Technol Dec. 2005;16(12):R93–R110.
[13] Rahimi-Eichi H, Ojha U, Baronti F, Chow M-Y. Battery management system: an overview of its application in the smart grid and electric vehicles. IEEE Ind Electron Mag 2013;7(2):4–16.
[14] Xia B, Zhao X, de Callafon R, Garnier H, Nguyen T, Mi C. Accurate Lithium-ion battery parameter estimation with continuous-time system identification methods. Appl Energy Oct. 2016;179:426–36.
[15] Wei Z, Lim TM, Skyllas-Kazacos M, Wai N, Tseng KJ. Online state of charge and model parameter co-estimation based on a novel multi-timescale estimator for vanadium redox flow battery. Appl Energy 2016;172:169–79.
[16] Duong V-H, Bastawrous HA, Lim K, See KW, Zhang P, Dou SX. Online state of charge and model parameters estimation of the $LiFePO_4$ battery in electric vehicles using multiple adaptive forgetting factors recursive least-squares. J Power Sources 2015;296:215–24.
[17] Dai H, Xu T, Zhu L, Wei X, Sun Z. Adaptive model parameter identification for large capacity Li-ion batteries on separated time scales. Appl Energy 2016;184:119–31.
[18] Tong S, Klein MP, Park JW. On-line optimization of battery open circuit voltage for improved state-of-charge and state-of-health estimation. J Power Sources 2015;293:416–28.
[19] He H, Xiong R, Guo H. Online estimation of model parameters and state-of-charge of $LiFePO_4$ batteries in electric vehicles. Appl Energy 2012;89(1):413–20.
[20] Berecibar M, Devriendt F, Dubarry M, Villarreal I, Omar N, Verbeke W, Van Mierlo J. Online state of health estimation on NMC cells based on predictive analytics. J Power Sources 2016;320:239–50.
[21] Chen Z, Mi CC, Fu Y, Xu J, Gong X. Online battery state of health estimation based on Genetic Algorithm for electric and hybrid vehicle applications. J Power Sources 2013;240:184–92.
[22] Fleischer C, Waag W, Heyn H-M, Sauer DU. On-line adaptive battery impedance parameter and state estimation considering physical principles in reduced order equivalent circuit battery models: Part 1. Requirements, critical review of methods and modeling. J Power Sources 2014;260:276–91.
[23] Howey DA, Mitcheson PD, Yufit V, Offer GJ, Brandon NP. Online measurement of battery impedance using motor controller excitation. IEEE Trans Veh Technol 2014;63(6):2557–66.
[24] Alavi SMM, Birkl CR, Howey DA. Time-domain fitting of battery electrochemical impedance models. J Power Sources 2015;288:345–52.
[25] Verbrugge M, Frisch D, Koch B. Adaptive energy management of electric and hybrid electric vehicles. J Electrochem Soc 2005;152(2):A333.
[26] Verbrugge M, Koch B. Generalized recursive algorithm for adaptive multiparameter regression. J. Electrochem. Soc. 2006;153(1):A187.
[27] Verbrugge M. Adaptive, multi-parameter battery state estimator with optimized time-weighting factors. J Appl Electrochem 2007;37(5):605–16.
[28] Juang LW, Kollmeyer PJ, Jahns TM, Lorenz RD. System identification-based lead-acid battery online monitoring system for electric vehicles. In: IEEE energy conversion congress and exposition 2010. p. 3903–10.
[29] Hu X, Sun F, Zou Y. Online model identification of lithium-ion battery for electric vehicles. J Cent South Univ Technol Oct. 2011;18(5):1525–31.
[30] Lee J, Kim Y, Cha H. A new battery parameter identification considering current, SOC and Peukert's effect for hybrid electric vehicles. In: IEEE Energy Conversion Congress and Exposition 2011. p. 1489–94.
[31] Wang S, Verbrugge M, Wang JS, Liu P. Multi-parameter battery state estimator based on the adaptive and direct solution of the governing differential equations. J Power Sources 2011;196(20):8735–41.
[32] Roscher MA, Bohlen OS, Sauer DU. Reliable state estimation of multicell lithium-ion battery systems. IEEE Trans Energy Convers Sep. 2011;26(3):737–43.
[33] Mandal LP, Cox RW. A transient-based approach for estimating the electrical parameters of a lithium-ion battery model. In: IEEE Energy Conversion Congress and Exposition 2011. p. 2635–40.
[34] Sabatier J, Aoun M, Oustaloup A, Grégoire G, Ragot F, Roy P. Fractional system identification for lead acid battery state of charge estimation. Sig Proc 2006;86(10):2645–57.
[35] Dai H, Wei X, Sun Z, Wang J, Gu W. Online cell SOC estimation of Li-ion battery packs using a dual time-scale Kalman filtering for EV applications. Appl Energy 2012;95:227–37.
[36] Plett GL. Sigma-point Kalman filtering for battery management systems of LiPB-based HEV battery packs: Part 2: Simultaneous state and parameter estimation. J Power Sources 2006;161(2):1369–84.
[37] Haifeng Dai, Xuezhe Wei, Zechang Sun. A new SOH prediction concept for the power lithium-ion battery used on HEVs. In: IEEE Vehicle Power and Propulsion Conference 2009. p. 1649–53.
[38] Xiong R., Sun F., Chen Z., He H. A data-driven multi-scale extended Kalman filtering based parameter and state estimation approach of lithium-ion polymer battery in electric vehicles; 2014.
[39] Do Dinh Vinh, Forgez C, El Kadri Benkara K, Friedrich G. Impedance observer for a li-ion battery using kalman filter. IEEE Trans Veh Technol 2009;58(8):3930–7.
[40] Zhang Q, White RE. Calendar life study of Li-ion pouch cells. J Power Sources 2007;173(2):990–7.
[41] Samadi MF, Alavi SMM, Saif M. Online state and parameter estimation of the Li-ion battery in a Bayesian framework. In: American Control Conference 2013. p. 4693–8.
[42] Xiong R, Yu Q, Wang LY, Lin C. A novel method to obtain the open circuit voltage for the state of charge of lithium ion batteries in electric vehicles by using H infinity filter. Appl Energy 2017.
[43] Chen C, Sun F, Xiong R, He H. A novel dual H infinity filters based battery parameter and state estimation approach for electric vehicles application. Energy Proc 2016;103:375–80.
[44] Fei Zhang, Guangjun Liu, Lijin Fang, A battery state of charge estimation method using sliding mode observer. In: 2008 7th world congress on intelligent control and automation; 2008, p. 989–994.
[45] Kim I-S. The novel state of charge estimation method for lithium battery using sliding mode observer. J Power Sources Dec. 2006;163(1):584–90.
[46] Zhang C, Wang LY, Li X, Chen W, Yin GG, Jiang J. Robust and adaptive estimation of state of charge for lithium-ion batteries. IEEE Trans Ind Electron Aug. 2015;62(8):4948–57.
[47] Forman JC, Moura SJ, Stein JL, Fathy HK. Genetic identification and fisher identifiability analysis of the Doyle–Fuller–Newman model from experimental cycling of a LiFePO4 cell. J Power Sources 2012;210:263–75.
[48] Schmidt AP, Bitzer M, Imre ÁW, Guzzella L, Model-based distinction and quantification of capacity loss and rate capability fade in Li-ion batteries; 2010.

[49] Moura SJ., Krstic M., Chaturvedi NA. Adaptive PDE Observer for Battery SOC/SOH Estimation. In: Volume 1: adaptive control; advanced vehicle propulsion systems; aerospace systems; autonomous systems; battery modeling; biochemical systems; control over networks; control systems design; cooperativ; 2012. p. 101–10.
[50] Klein R., Chaturvedi NA., Christensen J., Ahmed J., Findeisen R., Kojic A. State estimation of a reduced electrochemical model of a lithium-ion battery. In: Proceedings of the 2010 American control conference; 2010. p. 6618–23.
[51] Xing Y, He W, Pecht M, Tsui KL. State of charge estimation of lithium-ion batteries using the open-circuit voltage at various ambient temperatures. Appl Energy 2014;113:106–15.
[52] Smith K, Wang C-Y. Solid-state diffusion limitations on pulse operation of a lithium ion cell for hybrid electric vehicles. J Power Sources 2006;161(1):628–39.
[53] Widanage WD, Barai A, Chouchelamane GH, Uddin K, McGordon A, Marco J, Jennings P. Design and use of multisine signals for Li-ion battery equivalent circuit modelling. Part 2: Model estimation. J Power Sources 2016;324.
[54] Vörös J. An iterative method for hammerstein-wiener systems parameter identification. J Electr Eng 2004;55:11–2.
[55] Vörös J. Parameter identification of Wiener systems with multisegment piecewise-linear nonlinearities. Syst Control Lett Feb. 2007;56(2):99–105.
[56] Zhou L, Li X, Pan F. Least-squares-based iterative identification algorithm for Wiener nonlinear systems. J Appl Math May 2013;2013:1–6.
[57] Wang D, Ding F. Least squares based and gradient based iterative identification for Wiener nonlinear systems. Signal Processing May 2011;91(5):1182–9.
[58] Chaudhary NI, Raja MAZ. Identification of Hammerstein nonlinear ARMAX systems using nonlinear adaptive algorithms. Nonlinear Dyn 2015;79(2):1385–97.
[59] Aslam MS, Chaudhary NI, Raja MAZ. A sliding-window approximation-based fractional adaptive strategy for Hammerstein nonlinear ARMAX systems. Nonlinear Dyn. 2017;87(1):519–33.
[60] Barai A, Widanage WD, Marco J, McGordon A, Jennings P. A study of the open circuit voltage characterization technique and hysteresis assessment of lithium-ion cells. J Power Sources 2015;295:99–107.
[61] Roscher MA, Sauer DU. Dynamic electric behavior and open-circuit-voltage modeling of LiFePO4-based lithium ion secondary batteries. J Power Sources 2011;196(1):331–6.
[62] Verbrugge M, Tate E. Adaptive state of charge algorithm for nickel metal hydride batteries including hysteresis phenomena. J Power Sources 2004;126(1):236–49.
[63] Uddin K, Picarelli A, Lyness C, Taylor N, Marco J. An acausal Li-ion battery pack model for automotive applications. Energies 2014;7(9):5675–700.
[64] Ferguson TR. Lithium-ion battery modeling using non-equilibrium thermodynamics. Massachusetts Institute of Technology; 2014.
[65] Grens EA, Tobias CW. The influence of electrode reaction kinetics on the polarization of flooded porous electrodes. Electrochim Acta 1965;10(8):761–72.
[66] Widanage WD, Barai A, Chouchelamane GH, Uddin K, McGordon A, Marco J, Jennings P. Design and use of multisine signals for Li-ion battery equivalent circuit modelling. Part 1: Signal design. J Power Sources 2016;324.
[67] Ljung L. System identification. Theory for the user. Prentice-Hall; 1987.
[68] Honig ML., Messerschmitt DG. Adaptive filters: structures, algorithms, and applications. Kluwer; 1984.
[69] Garnier H., Wang L., Young PC. Identification of continuous-time models from sampled data: issues, basic solutions and relevance. In: Identification of continuous-time models from sampled data. London: Springer; p. 1–29.